Charged particle multiplicity in ^{28}Si + Al, Cu, and Pb reactions at E_{lab} = 14.6 GeV/nucleon

J. Barrette,[3] R. Bellwied,[6,*] P. Braun-Munzinger,[6] W. E. Cleland,[5] G. David,[6] O. Dietzsch,[10] E. Duek,[1,†] M. Fatyga,[1] D. Fox,[2,‡] S. V. Greene,[9] J. R. Hall,[4] R. Heifetz,[7] T. K. Hemmick,[9,§] M. Herman,[6,**] N. Hermann,[6,††] R. W. Hogue,[1] G. Ingold,[6,‡‡] K. Jayananda,[5] D. Kraus,[5] S. Kumar,[9] R. Lacasse,[3] D. Lissauer,[1] W. J. Llope,[6] T. Ludlam,[1] R. Majka,[9] D. Makowiecki,[1] S. K. Mark,[3] S. R. McCorkle,[1] J. T. Mitchell,[9] M. Muthuswamy,[6] E. O'Brien,[1] L. Olsen,[1,††] V. Polychronakos,[1] C. Pruneau,[3] M. Rawool-Sullivan,[8,§§] F. Rotondo,[9] J. Sandweiss,[9] J. Simon-Gillo,[8,§§] U. Sonnadara,[5] J. Stachel,[6] J. P. Sullivan,[8,§§] J. Sunier,[2] E. M. Takagui,[5] H. Takai,[1] T. Throwe,[1] H. van Hecke,[2] L. Waters,[6,§§] K. Wolf,[8] D. Wolfe,[4] C. L. Woody,[1] N. Xu,[6] and Z. Zhang[5]

(E814 Collaboration)

[1] *Brookhaven National Laboratory, Upton, New York 11973*
[2] *Los Alamos National Laboratory, Los Alamos, New Mexico 87545*
[3] *McGill University, Montreal, Canada H3A 2T8*
[4] *University of New Mexico, Albuquerque, New Mexico 87131*
[5] *University of Pittsburgh, Pittsburgh, Pennsylvania 15260*
[6] *State University of New York, Stony Brook, New York 11794*
[7] *University of Tel Aviv, Tel Aviv, Israel*
[8] *Texas A&M University, College Station, Texas 77843*
[9] *Yale University, New Haven, Connecticut 06511*
[10] *Universidade de São Paulo, São Paulo, Brazil*

(Received 12 November 1991)

Collisions of ^{28}Si+Al, Cu, and Pb at E_{lab}=14.6 GeV/nucleon were studied at the Brookhaven National Laboratory Alternating Gradient Synchrotron. Charged particle multiplicity was measured over the pseudorapidity interval $0.875 \leq \eta \leq 3.86$ with a silicon pad detector. A strong correlation is seen between the multiplicity and the transverse energy measured in the interval $-0.5 \leq \eta \leq 0.8$. Correlation with the energy going forward after the collision and comparison with calculations indicate that rescattering is required to explain the data. The data are compared under the assumption of Koba-Nielson-Olesen scaling. The measured multiplicity scales approximately with the total number of participant nucleons and less well with the available center-of-mass kinetic energy.

PACS number(s): 25.75.+r

I. INTRODUCTION

The relevance of the measurement of global observables to the understanding of relativistic nucleus-nucleus collisions has been summarized recently in Refs. [1] and [2]. Such data can provide information about the energy deposition and the degree of thermalization achieved in heavy-ion collisions. They can also be used to put tight constraints on the existing models which describe relativistic nucleus-nucleus collisions such as relativistic quantum molecular dynamics [3], string models [4–6], and other multiple collision models [7,8]. A survey of existing measurements is given in Ref. [1].

Experiment E814 is a fixed target relativistic heavy-ion experiment at the Brookhaven National Laboratory (BNL) Tandem–Alternating Gradient Synchrotron (AGS) accelerator complex. Among the goals of this ex-

*Present address: Dept. of Physics, Wayne State University, Detroit, MI 48202.
†Present address: SSC Laboratory, MS 1070, 2550 Beckleymeade Ave., Dallas, TX 75248.
‡Present address: Indiana University Cyclotron Facility, 2401 Milo B. Sampson Lane, Bloomington, IN 47405.
§Present address: State University of New York, Stony Brook, NY 11794.
**Present address: Johns Hopkins Oncology Center, Baltimore, MD 21205.
††Present address: Physikalisches Institut, Universität Heidelberg, D 69 Heidelberg, Germany.
‡‡Present address: Brookhaven National Laboratory, Upton, NY 11973.
§§Present address: Los Alamos National Laboratory, Los Alamos, NM 87545.

periment are the investigation of global features of central collisions between ^{28}Si projectiles of $E_{\rm lab}$ = 14.6 GeV/nucleon and a range of target nuclei. The global variables which are measured in this experiment include transverse energy, E_t, over nearly the full solid angle, charged particle multiplicity, N_c, in the forward hemisphere, and the zero-degree energy, E_0 (further described below). First results on transverse energy production [9] into the backward hemisphere ($\theta_{\rm lab} > 45°$) and its correlation with forward going nucleons measured in a cone angle of approximately 0.8° centered at $\theta_{\rm lab} = 0°$ provided evidence for a considerable amount of energy deposition ("stopping") in central Si-nucleus collisions. Furthermore, the observed strong dependence on target mass of the produced transverse energy [9] can only be understood if particles created in the collision (mostly pions) are allowed to interact with the participant and spectator matter of the collision ("rescattering"). In this paper we present new experimental results on the distribution of charged particles in Si-nucleus collisions and their correlation with observables whose measurement was reported in Ref. [9]. A preliminary account of our data has been reported in Ref. [10].

In Sec. II a brief overview is given of the experiment. Section III describes in detail the silicon pad detectors used to measure the charged particle multiplicity distributions including a discussion of all the corrections applied to the raw data. In Sec. IV we present our results for the three targets studied. The data are compared to predictions from a multiple collision model and their correlation with transverse energy and forward energy is discussed. A summary and conclusion is given in Sec. V.

II. EXPERIMENTAL SETUP

A schematic diagram of the E814 apparatus is shown in Fig. 1. The target is surrounded by calorimeters; the participant calorimeter (PCAL) covers the forward hemisphere (pseudorapidity interval $0.83 \leq \eta \leq 4.20$) and the target calorimeter (TCAL) covers the backward hemisphere ($-0.9 \leq \eta \leq 0.8$, averaged in azimuth and including the back wall). The charged particle multiplicity is

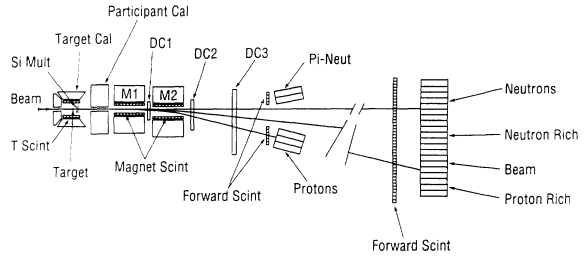

FIG. 1. Diagram of the E814 experiment. The beam enters through a hole in the back wall of the target calorimeter. Forward going particles pass through the participant calorimeter opening and magnets M1 and M2 which provide the deflection for the forward spectrometer. Track positions are measured in drift chambers DC1, DC2, and DC3. Charge is measured in the forward scintillators and energy is measured in the U/Cu calorimeters. The drawing is not to scale.

measured with the silicon pad detectors located downstream of the target and inside of the TCAL. Particles passing through a rectangular hole in the PCAL with opening angles of 12 msr (vertically) and 18 msr (horizontally) and centered at 0° are measured in the forward spectrometer. This spectrometer combines high precision track measurement in the drift/pad detectors [11] DC1, DC2, and DC3 with charge information from the forward scintillator hodoscopes and total energy measurements from the U/Cu/Sci sampling calorimeters (UCAL) [12]. The total energy measured in the UCAL of all particles passing through the PCAL aperture and magnets M1 and M2 defines the zero-degree energy (E_0). Most of these particles are beam rapidity baryons; particles of less rigidity are swept away by magnets M1 and M2. More detail about the experimental apparatus can be found in Sec. IV and Refs. [9] and [13].

A fast pretrigger for the data aquisition system was generated by the coincidence of a valid beam particle (as defined by the coincidence of beam scintillators located upstream of the target) and a minimum number of hits in either the multiplicity counter or the scintillator paddles which line the inside of the TCAL. To form the second level trigger, E_t data from the side walls of the TCAL and the raw charged particle multiplicity were each discriminated at three different thresholds and the results appropriately downscaled so as to obtain comparable statistics across the whole range of measured N_c and TCAL E_t. For each accepted event all trigger information was written to tape to allow accurate reconstruction of the measured spectra.

To eliminate pileup effects, only events separated from a previous or following beam particle by at least 1 μs were written to tape. Events in which this separation was smaller than the time resolution of our electronics ($\approx$ 30 ns) were eliminated during off-line analysis by using the pulse height data from the beam defining scintillators. Additional triggers (subject to the timing cut above) were generated either at random or by the beam itself for the purposes of measuring backgrounds, efficiencies, and ADC pedestals.

III. E814 MULTIPLICITY DETECTOR

The charged particle multiplicity detector in E814 consists of two silicon pad detectors. Each pad detector is made from a disk of silicon 300 μm thick and approximately 38 mm in radius. The active region of each pad detector extends to a maximum radius of 34 mm and is divided into 512 pads. Detector 1 is segmented into 8 concentric rings of 64 pads each and detector 2 is segmented into 12 concentric rings of from 16 to 64 pads as shown in Fig. 2. The detectors cover the pseudorapidity (η) interval from 3.86 to 0.88 (2.4° to 45.3° in the laboratory) in 20 steps and are placed relative to the target as shown in Fig. 3.

The read-out electronics for the multiplicity detector consists of a preamplifier and a level discriminator for each detector element. This system only registers whether or not each individual pad records a signal above threshold for a given event. It does not indicate if the

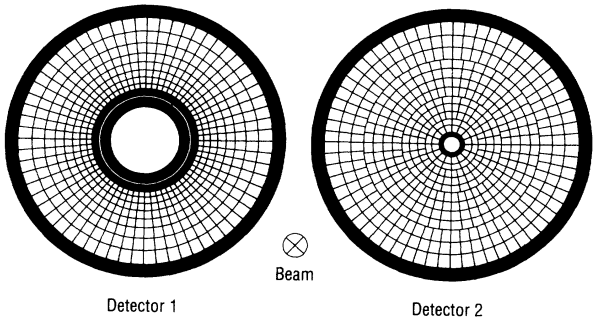

FIG. 2. Pad segmentation of the E814 silicon multiplicity detectors. Each of the detectors has 512 pads.

pad was hit by more than one particle. The discriminator thresholds were set to a value equivalent to approximately one-half of the energy loss (most probable) of a minimum ionizing particle, at normal incidence, in 300 μm of silicon. An analysis using data from a subset of the pads connected to ADCs and using measured discriminator efficiency curves shows that, for Si+Pb collisions, there is a slight excess of low energy signals as compared to a Landau distribution. However, this excess amounts to less than one percent of the total multiplicity and is reduced overall when certain noisy channels and background events are removed from the sample. The hit multiplicity from electronic noise was measured to be much less than one hit per event as determined by random strobing of the detector during the experiment.

The multiplicity detector is sensitive to low energy charged particles as the detector will register any particle depositing more than $\approx$40–60 keV in a pad. There are only a few centimeters of air, 0.5 mm of G10 board, and the target material itself between the point of collision and the detector's silicon. In the worst case (traversing all material from the front of the target to the silicon at the largest possible angle) a proton would require a minimum kinetic energy of slightly more than 27 MeV to be detected in the front detector and just more than 24 MeV to reach the back detector. These values are small considering that the center-of-mass relativistic γ for a central Si+Pb collision is 1.26 and that the detector is at forward angles. Not only does the detector record charged reaction products with high efficiency but energetic target spectator fragments as well.

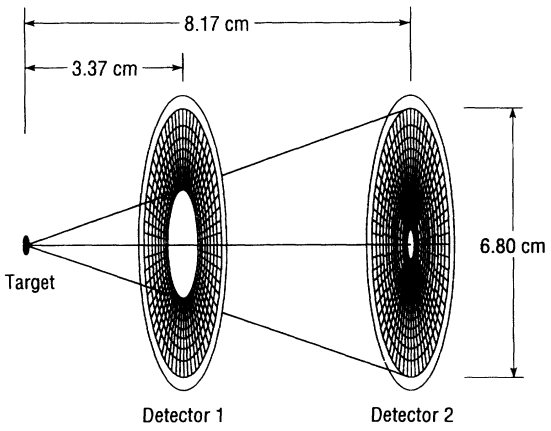

FIG. 3. Position of the silicon detectors relative to the target. They cover the pseudorapidity interval from 3.86 to 0.875. There is no overlap of the active regions of the two detectors.

At any one time from eight to ten percent of the pads of the multiplicity detector were not functional. The combined effect of "bad" pads and multiple occupancy is to cause the mean multiplicity measured with the detector to be less than the "true" multiplicity by eight percent for low multiplicity events to as much as twenty percent for events of high multiplicity. The multiplicity cross section distributions shown below ($d\sigma/dN_c$) have been corrected to first order for the effects of both bad pads and multiple event occupancy of any single pad. By first order we mean a rescaling of the data (event by event) for the number of dead pads in each ring (correcting ring by ring takes into account the effects of the variation of multiplicity with pseudorapidity) and the mean ring multiple occupancy at a given total multiplicity (determined from our $dN_c/d\eta$ data shown below). The "bad" pads (either very noisy or giving no response) are identified from an ensemble of events by demanding azimuthal symmetry in each ring with an allowance for beam offset and non-normal beam incidence. The correction for multiple occupancy is determined from the ensemble by assuming Poisson statistics for each ring. At a given measured total multiplicity, the correct per pad multiplicity (μ) in a ring is determined from the measured probability of not having a hit in a pad of that ring [$P_\mu(0) = e^{-\mu}$]. At the highest multiplicity and at the most forward angles the correction for multiple occupancy is as much as twenty percent but it is much smaller at larger angles where there are more pads in each ring.

The accuracy of the corrections for bad pads and multiple occupancy was investigated and results are shown in Fig. 4. Here events from a HIJET event generator [8] were allowed to produce hits in the simulated multiplicity detector which was given a typical number of bad pads. As can be seen in Fig. 4, when the correction procedure described above is applied to the Monte Carlo data, the derived $d\sigma/dN_c$ spectrum is virtually identical to the known input spectrum. A discrepancy between the input and corrected spectra is seen where the cross section starts to fall; here the corrected data lie slightly below the input data and their falloff is less abrupt. It should be noted that, while the above correction procedure assumes that the data obey Poisson statistics, the actual data may contain events with spatially correlated particles. However, because of the small pad sizes, such effects are believed to be small.

The multiplicity data are also corrected for the contribution from delta rays produced in the target. The measured $dN/d\eta$ spectra of delta rays produced in each of the various targets by a noninteracting Si projectile are virtually identical in shape. Only for the Pb target is a small difference observed (see Fig. 5). The mean mea-

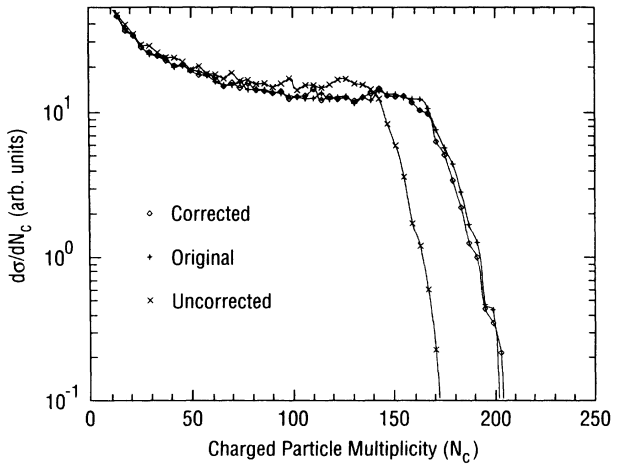

FIG. 4. Results of the combined correction procedures for dead pads and multiple occupancy. The curve labeled as "original" is from a HIJET event generator. The curve labeled "uncorrected" is the response to the "original" events of a theoretical E814 multiplicity detector with an average number of dead pads. The curve labeled "corrected" is the result of applying the correction procedure to the "uncorrected" data.

sured delta ray multiplicities depend both on the target and its thickness; for the various targets the measured multiplicities are 4.04 (Al, 327 mg/cm^2), 5.67 (Al, 647 mg/cm^2), 4.66 (Cu, 595 mg/cm^2), and 4.34 (Pb, 1110 mg/cm^2). To obtain a correction to the multiplicity distributions from delta-ray production we use the measured delta ray spectrum ($dN/d\eta$) of a Si projectile, weighted by a factor of

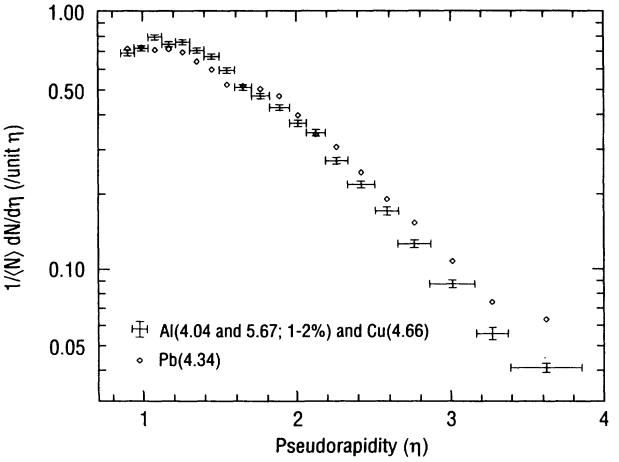

FIG. 5. Normalized $dN_c/d\eta$ distributions for delta rays generated by the passage of the Si beam through the different targets. Al and Cu targets produce virtually the same distribution of delta rays while that from Pb target is only slightly different. In the lower left hand corner of the figure are given the mean delta-ray multiplicity for each target.

$$0.5(1.0 + \text{mult}/196). \quad (1)$$

The measured spectrum is used for Pb, while for the Al and Cu targets the spectrum from the mean of the spectra measured for those targets is used. The factor 0.5 in Eq. (1) appears because an interacting Si projectile survives on average only one-half of the way through the target. The remaining terms estimate the delta ray production after the collision by assuming that the charged ejectiles will produce the same spectrum of delta rays as the projectile but that almost every ejectile has only a charge of one. Here mult is the measured N_c of the event and 196 equals Z^2_{Si}. Because the targets were thin, the resulting correction is small.

Next the data were corrected for the in-target conversion of π^0 decay gamma rays to e^+/e^- pairs. For the Pb and Cu targets Monte Carlo studies using the HIJET event generator [8] and the GEANT [14] tracking package were used to determine, as a function of N_c, not only the number of e^+/e^- pairs produced but also their angular distributions (including multiple scattering effects). At each multiplicity a constant fraction of the produced pairs hit in a single pad of the multiplicity detector where, because of their correlation, they are registered as a single hit. For the Pb and Cu targets the resulting corrections are a constant 6.8% and 1.4% of the measured multiplicity, respectively. The correction for Al is negligible.

An additional correction to the multiplicity data is due to the charge sharing that takes place when a particle hits the detector in a region between two pads. Previous investigations [15] have shown that in this case there is no loss of charge but rather that the charge is shared between the two adjacent pads. The degree of sharing depends upon the exact position of the hit and angle of the particle. Depending on the discriminator setting, the sharing of charge between pads can result in the hit being registered in neither of the pads, in only one of the pads, or in both of the pads. Using a simple geometric model we have calculated, for each ring, the effective area of sharing for which either the hit is completely lost or counted twice. The results are insignificant for the inner rings but a 1–2 % effect is calculated for the outer rings. For equal ring occupancy this would imply only a 0.5% correction to the total multiplicity. For the purposes of this paper this correction can safely be neglected.

An illustration of the sizes of the different corrections is given in Table I for the Si+Pb system at high multiplicity.

TABLE I. Typical corrections to the multiplicity for Si+Pb having an initial multiplicity of 150. This corresponds to about a factor of 4 down from the $d\sigma/dN_c$ plateau. The last column gives the resulting multiplicity after the corrections are successively applied.

	Correction	N_c
Raw data		150
Dead pads	$\approx +8\%$	162
Multiple occupancy	$\approx +9\%$	177
Delta rays	-4.1	173
Converted π^0 gamma rays	-11.8	161
Charge sharing	< -1	161

For Pb the final data and the data corrected just for bad pads lie virtually on top of one another. The slopes of the two curves beyond the plateau are identical but the transition from plateau to slope is slightly flatter in the final data as compared to the data corrected only for pad response.

IV. EXPERIMENTAL RESULTS

The data discussed in this paper were taken in June of 1989 and 1990 at the BNL AGS with an $E_{\rm lab}$ = 14.6 GeV/nucleon ^{28}Si beam on targets of natural Al, Cu, and Pb. Each of the targets had a thickness corresponding to 1.2% of a nuclear interaction length (a 2% Al target was also used) for the interacting Si projectile. In the 1989 data there is a small contamination from events in which the beam interacts in the front silicon detector (see Figs. 2 and 3). This causes a small discontinuity to occur in the $dN_c/d\eta$ spectra at the junction of the inner ring of the front multiplicity detector and the outer ring of the back multiplicity detector (see Fig. 3). For the 1990 measurements the hole inside of the active region of the front multiplicity detector for the passage of the beam was enlarged to reduce this problem. During the 1990 run the whole detector was noisier than during the 1989 run. The data from the two runs are otherwise in very good agreement.

Unless otherwise stated the trigger for the data presented in this paper is from the multiplicity detector itself. Events with reconstructed multiplicities (for all targets) above about 30 are free from first level multiplicity trigger bias. Events with smaller multiplicities are accepted with decreasing efficiency until a minimum multiplicity of about 20 below which no events were accepted. Data with charged particle multiplicities less than the above values (see Fig. 6) were obtained by including beam trigger events which were taken concurrently with the other data.

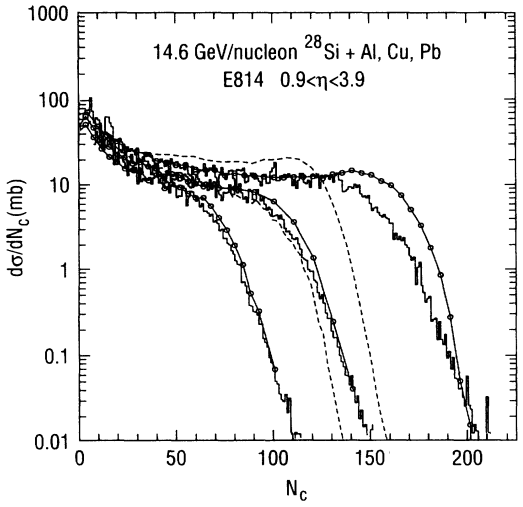

FIG. 6. Comparison of measured multiplicity distributions, $d\sigma/dN_c$, for a beam of ^{28}Si on targets of Al, Cu, and Pb with the predictions from a HIJET event generator. The dashed curves were generated from HIJET without rescattering for each of the targets. The curve with circles was generated using HIJET with rescattering. For Al these two curves overlap.

The corrected measured multiplicity cross section distributions, $d\sigma/dN_c$, for the three targets are shown in Fig. 6. These distributions have been corrected for empty-target-frame events which only significantly affect the data below multiplicities of 40. There is an estimated systematic uncertainty of the order of 6–8 % in the measured cross sections for each of these targets. The uncertainty in the corrected multiplicity from the multiplicity corrections discussed above is estimated to be of the order of ±4–6 channels at the multiplicity shown in Table I for the Pb data. This estimate was derived after comparing the results from different runs.

In Fig. 6 note the strongly increasing multiplicity with the increasing mass of the target, corroborating a trend already observed in transverse energy production [9] into the backward hemisphere. In order to put these results into perspective we also show, in Fig. 6, the results of calculations made using the HIJET event generator. The dashed lines are from HIJET with its standard parameters while the solid lines with open circles are from HIJET with rescattering included. We used the prescription [16] of Longacre and Shor without any change in parameters to include rescattering in the HIJET event generator. For Al the two HIJET curves lie on top of one another and are in excellent agreement with the data. For Cu both HIJET curves are also in good agreement with the data; standard HIJET agrees very well with the data until about an order of magnitude down from the plateau where HIJET with rescattering better matches the data. While good agreement is observed for the lighter targets, the standard HIJET event generator produces far fewer particles than are experimentally observed for the Pb target. Multiplicity curves generated using the FRITIOF [5] and the Landau fireball [17] models show a very similar trend, falling well short of the observed multiplicities for the Pb target. Better agreement between the Pb data and the calculations is found if one takes into account the possibility that produced particles may rescatter in the participant and spectator matter as is shown by the solid curve with open circles in Fig. 6. In the calculations this rescattering produces virtually no change for Si+Al and only a small change for Si+Cu but leads to a large increase in multiplicity for Si+Pb. A similar conclusion is reached in Ref. [9] for the transverse energy measured in the target calorimeter (the NaI calorimeter surrounding the target region and subtending from 45° to 175° in the laboratory). There also the transverse energy distribution, E_t, for the Pb target is much better described by a HIJET calculation in which rescattering is included. The transverse energy calculations for Al and Cu are much less sensitive to the inclusion of rescattering.

In Fig. 7 a contour plot of the charged particle multiplicity versus the transverse energy in the TCAL is shown for the Pb target using a minimum bias trigger. Even though the two detectors cover very different regions of

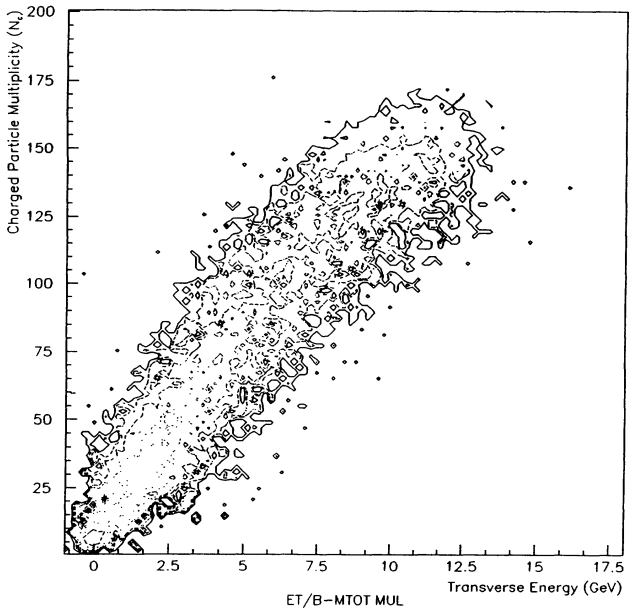

FIG. 7. Correlation of the transverse energy seen in the TCAL detector and the charged particle multiplicity seen in the multiplicity detector. The contours in this plot are logarithmic. These two detectors cover different ranges of pseudorapidity.

pseudorapidity, there is a very strong correlation between the number of charged particles going forward into the multiplicity detector and the amount of transverse energy going backwards. This strong correlation indicates that the changes seen in both multiplicity and transverse energy are not the result of large fluctuations in the sharing of energy between the forward and backward directions but rather that the increases are taking place simultaneously. Only for the largest multiplicities or transverse energies can one see an indication of the competition for the energy production between the forward and backward directions; the shape of the correlation then depends on whether one triggers the data in the backward hemisphere (transverse energy trigger) or forward hemisphere (multiplicity trigger).

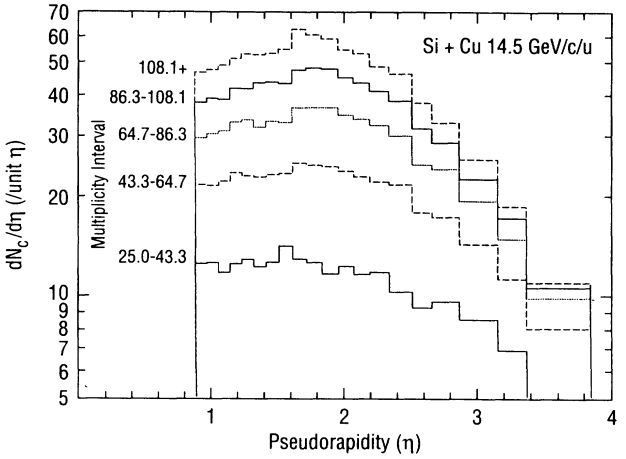

FIG. 9. $dN_c/d\eta$ for various multiplicity cuts in the data from the Cu target.

In Figs. 8–10, the evolution of $dN_c/d\eta$ as a function of the total multiplicity is shown for the various targets. These spectra are corrected for pad efficiency, multiple occupancy, delta rays, and π^0 gamma-ray conversion as explained above. Because these corrections are now applied as a function of η, the systematic error in a given η interval is estimated to be of the order of 10–12 %. For any given target the $dN_c/d\eta$ spectra were obtained by cutting on different intervals in N_c (Fig. 6) as indicated in the figures. The first interval, 25–43, is the only interval for which the the empty-target-frame correction was of any noticeable effect. The positions of these intervals can be related to the geometric cross section using Table II where are listed for each of the targets the approximate lower thresholds in the multiplicity spectrum necessary to obtain various percentages of the integrated measured cross section relative to the total geometric cross section.

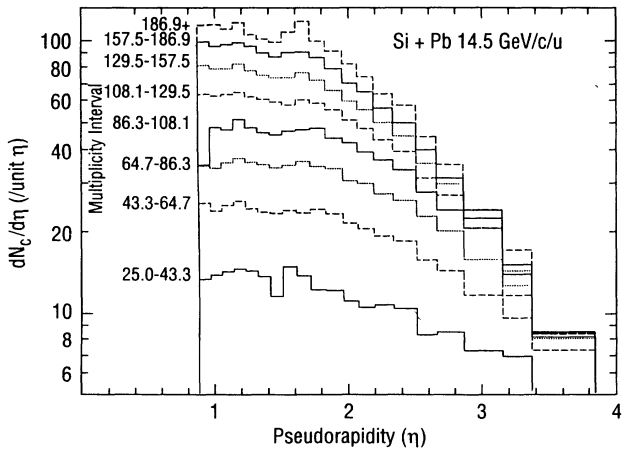

FIG. 8. $dN_c/d\eta$ for various multiplicity cuts in the data from the Pb target.

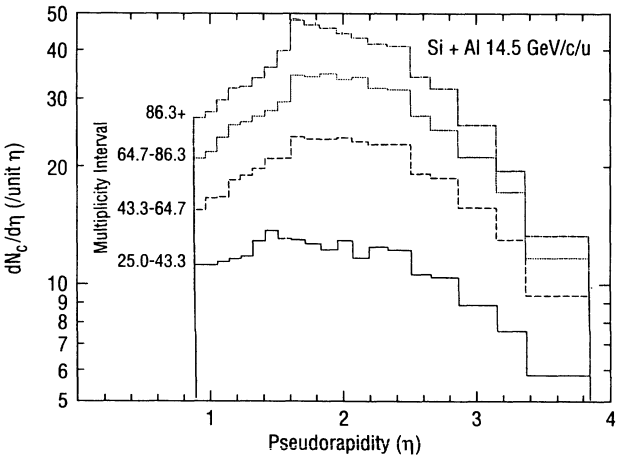

FIG. 10. $dN_c/d\eta$ for various multiplicity cuts in the data from the Al target.

TABLE II. Approximate lower thresholds in the multiplicity spectrum to obtain an integrated cross section of a given percentage relative to the total geometric cross section. The geometric cross section was calculated assuming the radius of each nucleon to be $1.2A^{1/3}$ fm.

σ/σ_{geo} (%)	Al	Cu	Pb
50	12	31	37
33	20	46	57
25	41	61	80
10	49	77	122
7	57	85	131
5	61	91	138

The geometric cross section was calculated assuming the radius of each nucleon to be $1.2A^{1/3}$ fm. Each of these $dN_c/d\eta$ spectra are approximately Gaussian. For Al and Cu the maxima of the distributions are well within the detector's acceptance while for Pb the distribution peaks near the edge of our detector's acceptance. The shift of the centroid of the distribution to smaller values of pseudorapidity with increasing target mass is expected from kinematics.

In Fig. 11 $dN_c/d\eta$ spectra gated on the upper 7% of the total inclusive cross section for each of the three targets are shown together with calculations for Pb from HIJET with rescattering (solid line) and from HIJET without rescattering (dotted line). In this figure the shift of the centroid of the multiplicity distributions with the mass of the target can clearly be seen. For Pb the calculation without rescattering fails to give enough multiplicity at the lowest rapidities and is clearly peaked forward of the data. The agreement with the calculation that does include rescattering is quite satisfactory.

To better understand the different $dN_c/d\eta$ distributions, a series of such spectra derived from narrow slices

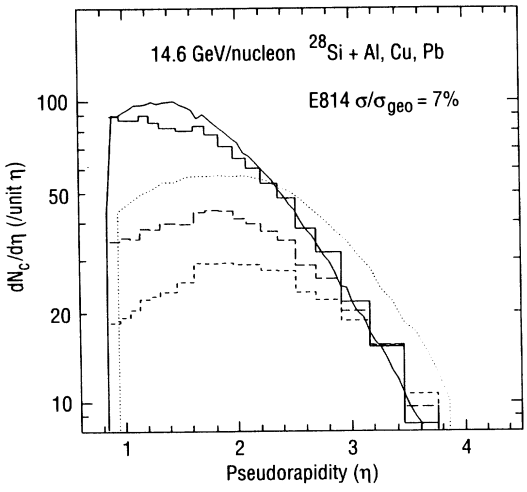

FIG. 11. $dN_c/d\eta$ for the upper 7% of the geometric cross section of each of the targets. The dotted curve is from a HIJET calculation that does not contain rescattering while the solid line is from a HIJET calculation that does contain rescattering.

($\Delta N_c = 5$) in the multiplicity spectra of each of the targets were fitted with Gaussian distributions (three parameter fits). For all targets reasonable fits to the data were obtained; however, the $dN_c/d\eta$ distributions are not exactly Gaussian and the deviation from Gaussian is greater at large η (see also Figs. 15 and 16). Multiple fits were made to progressively smaller η intervals of each data slice to determine the stability of the fit parameters. The results are presented in Figs. 12 and 13. The errors shown were derived from the difference between the minimum and maximum values of the parameters determined from the multiple fits.

In Fig. 12 the centroids of the Gaussian fits to the data (as described above) for each of the three targets are plotted against the mean multiplicity of the data. Note first that the pseudorapidity (η) of the centroids for Al and Cu are larger than the center-of-mass rapidity ($Y_{c.m.}$) that one would predict from the simple assumption that the projectile bores a hole of its own size through the center of the target nucleus. The calculated values of $Y_{c.m.}$ using this assumption are 1.74, 1.49, and 1.26 for the Al, Cu, and Pb targets, respectively. In contrast the centroids for the Pb distributions are actually smaller than this calculated $Y_{c.m.}$. The translation from rapidity (Y) to pseudorapidity (η) is, however, dependent on the particle's transverse mass (m_t) and transverse momentum (P_t),

$$\eta = \frac{1}{2}\ln\left[\frac{\sqrt{(m_t\sinh Y)^2 + P_t^2} + m_t\sinh Y}{\sqrt{(m_t\sinh Y)^2 + P_t^2} - m_t\sinh Y}\right]. \quad (2)$$

Furthermore, for a boost along the beam axis where P_t remains constant,

$$d\eta/dY = \frac{m_t\cosh Y}{\sqrt{(m_t\sinh Y)^2 + P_t^2}} = E/P = 1/\beta. \quad (3)$$

These equations show that the measured pseudorapidity of all massive particles will be larger than their true rapidity, with the difference being the largest for those particles having the smallest velocities. Thus, in the lab-

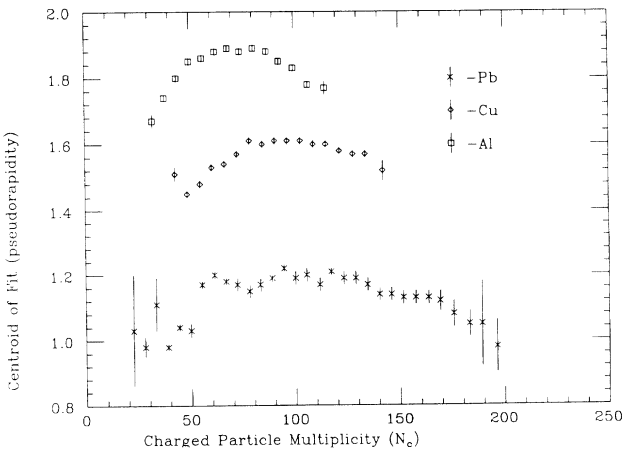

FIG. 12. Centroids of Gaussian fits to the $dN_c/d\eta$ spectra as a function of the multiplicity of the event.

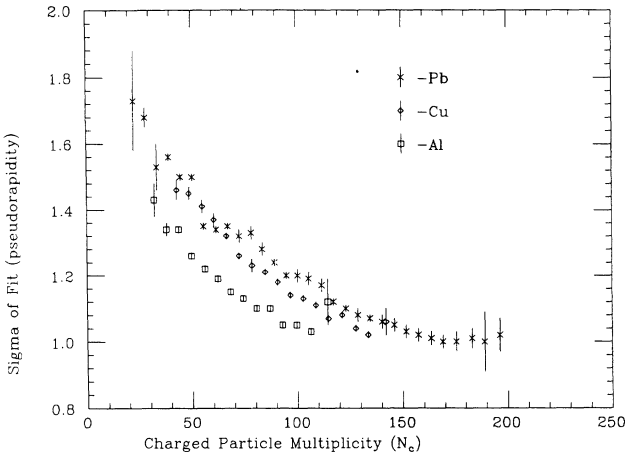

FIG. 13. Variance of the Gaussian peak fit to the $dN_c/d\eta$ spectra as a function of the multiplicity of the event.

oratory frame, the centroid of the measured particle distribution from a heavy-ion collision should be at a pseudorapidity greater than the effective $Y_{\text{c.m.}}$ of the collision. However, from Eq. (3) we know that when any particle of an initial rapidity and transverse momentum is given a boost such that its relativistic beta approaches one, then any additional boost that it is given (ΔY) will result in an almost equal change in its pseudorapidity ($\Delta\eta$). If the relative composition (particle mix, P_t, etc.) of two different distributions is about the same then the difference between the pseudorapidities of the centroids of those distributions should be about the same as the difference between their center-of-mass rapidities. Keeping this in mind, note that the curves for Al and Cu in Fig. 12 are spaced relative to each other by nearly what one would predict from the simplistic projectile plus core $Y_{\text{c.m.}}$ described above. As noted above this does not hold for Pb where the measured centroids of the fits are at a pseudorapidity smaller than $Y_{\text{c.m.}}$. Perhaps this indicates that for Pb there is a larger contribution from target spectators. Target spectators might also help explain the low multiplicity trend of the fit centroids of all targets to go to small values of η as the multiplicity gets smaller. In Fig. 11 we have noted for Pb that there is an excess of multiplicity in the data at small pseudorapidity as compared to calculations without "rescattering." This excess of events is consistent with the above results as it will move the centroid of the fits to smaller values of pseudorapidity.

In Fig. 13 we see the general trend of the widths of the distributions to get smaller as the multiplicity of the event gets larger. This can also be seen in Figs. 8–10 where at forward angles ($\eta > 2.8$), the differential multiplicity increases only very weakly with increasing total multiplicity while at the larger angles the differential multiplicity increases much more rapidly as more central events are selected. These results are consistent with the systematics presented in Refs. [1] and [18].

The data reported here agree very well with preliminary pseudorapidity distributions reported by the E802 Collaboration [19] for Si+Au collisions. Futhermore, the number of charged particles produced also agrees quantitatively with what is predicted by event generators such as HIJET, where essentially complete stopping of the projectile is assumed. As recently pointed out [20], however, identified particle spectra for pions and protons as measured by the E802 Collaboration [21] exhibit considerably less cross section near central rapidity than is predicted by such models. An interesting possibility is that this discrepancy could in part be due to an enhancement of particles at low transverse momentum which would be detected in our experiment but which could not be detected by the E802 spectrometer.

In Fig. 14 plots showing the correlation between the charged particle multiplicity N_c and the detected zero-degree energy E_0 are presented. In these plots we see that the Al, Cu, and Pb nuclei (each nucleus being progressively larger) produce progressively more multiplicity per unit of energy (nucleons) consumed in the collision, even though the multiplicity detector has a more favorable kinematic acceptance for lighter targets. Furthermore, we observe a large range of multiplicity leading to $E_0 \approx 0$ for the Pb target, a shorter range for the Cu target, and a very restricted range for the Al target which rarely attains complete overlap with the Si projectile. The ratios of the $d\sigma/dE_0$ spectra for the various targets are (allowing for trigger bias) what one would predict from the simple occultation of the beam nucleus by a totally absorbing target nucleus. That is to say, to the degree of resolution of interest here, at AGS energies E_0 is just a measure of the physical overlap of the projectile and the target nuclei and to first order $d\sigma/dE_0$ is purely geometric. In contrast, a trigger based on N_c (or E_t) is more correlated with the products of the reaction and hence the dynamics of the collision itself.

In Fig. 15 we show multiplicity data from several pseudorapidity intervals of each target as a function of the

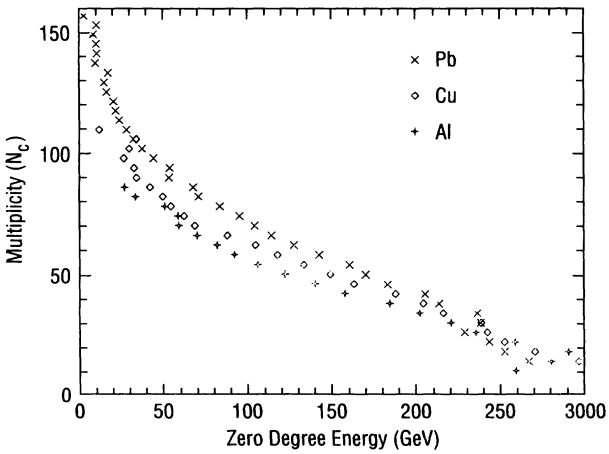

FIG. 14. Correlation between the measured charged particle multiplicity measured in the multiplicity detector and the zero-degree energy as measured by the downstream uranium calorimeters. The data were taken with an E_t trigger and the figure made by projecting on the multiplicity axis.

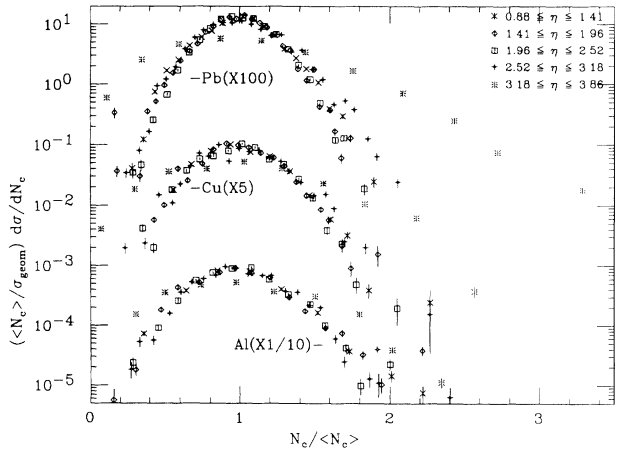

FIG. 15. Observed multiplicity distributions, plotted in KNO variables for each target at various pseudorapidity intervals. The distributions are virtually identical except for the most forward ($3.18 \leq \eta \leq 3.86$) interval where the distribution is wider for all three targets.

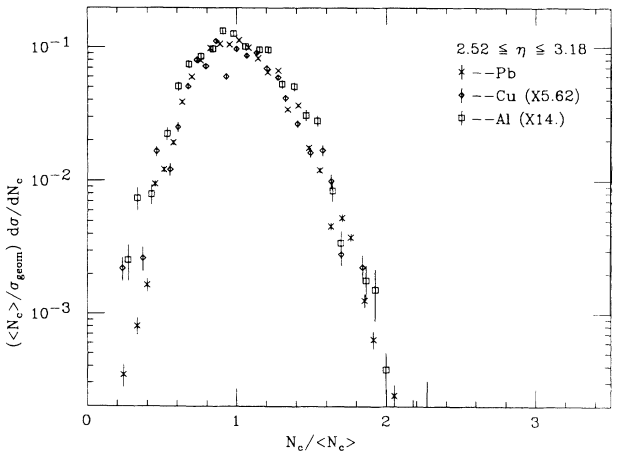

FIG. 16. Relative multiplicity distributions, plotted in KNO variables from the three targets at the same pseudorapidity interval.

KNO [22] variable $N_c/\langle N_c \rangle$, where N_c is the charged particle multiplicity of the event in that pseudorapidity interval and $\langle N_c \rangle$ is the average charged particle multiplicity of the events in that interval. For the Pb and Cu data, we select events in which all projectile nuclei interact by requiring that the zero-degree energy be less than 10 GeV, well below that of a single nucleon in the projectile. For the Al data, this cut is relaxed to 25 GeV, because for this target the probability for all nucleons in the projectile to interact is very small. All of the multiplicity distributions have practically the same shape, Gaussian with a slight tail, except for the most forward interval ($3.18 \leq \eta \leq 3.86$) where the distribution is much wider for all three targets. In Fig. 16 the relative distributions of the three targets for the same pseudorapidity interval ($2.52 \leq \eta \leq 3.18$) are compared. The three multiplicity distributions are very similar at this pseudorapidity interval, as are the distributions at each of the other intervals including the most forward interval where the distributions become wider. The Cu data are scaled relative to the Pb data by the relative areas of total overlap of the Si projectile with the target nuclei. The Al data, having a less restrictive zero-degree-energy requirement, are given an arbitrary scaling to match the other distributions.

At AGS energies, scaling in these variables appears to be satisfied for the targets investigated except at the most forward pseudorapidity interval where all three targets produce a wider distribution. This may be compared with emulsion data [23] from CERN taken at higher energy, using three different projectile-energy combinations, and having a similar but less restrictive centrality criterion. There the scaling among pseudorapidity intervals (inclusive) holds for a given projectile and energy but the distributions are different for the different beams.

Finally, in Figs. 17 and 18 we show the charged particle multiplicity in an equally large pseudorapidity interval of the forward hemisphere (the pseudorapidity interval from $\eta = Y_{\text{c.m.}}$ to $\eta = Y_{\text{c.m.}} + 2.12$) for each of the three targets. Using this interval reduces the contribution to the measured multiplicity from target spectator fragments. In these figures the horizontal axis is scaled for each of the targets by the impact-parameter-equals-zero value of either the center-of-mass kinetic energy, T_f (Fig. 17), or the impact-parameter-equals-zero number of nucleons [24], N_{tot}, involved in the collision (Fig. 18). The quantities $Y_{\text{c.m.}}$, T_f, and N_{tot} are calculated using the simple assumption that the projectile bores a hole of its own diameter through the target (inverted for the Al target). If the data were linearly related to the free dynamic values of either T_f or N_{tot}, then the scaled curves should all end at the same location on the horizontal axis of the appropriate figure. In Fig. 17 the data do not scale well with the so calculated available kinetic energy, T_f. This could imply that the transverse energy per particle from a central Si+Pb collision is smaller than that from

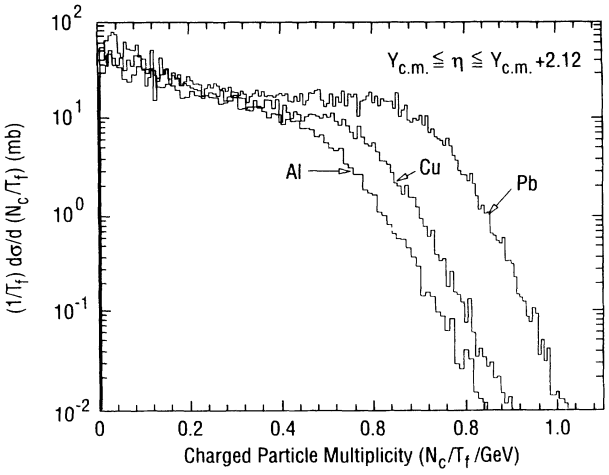

FIG. 17. $d\sigma/dN_c$ for a fixed interval in pseudorapidity relative to $Y_{\text{c.m.}}$ for each of the targets. The horizontal axis has been scaled by the maximum center-of-mass kinetic energy available for each of the targets.

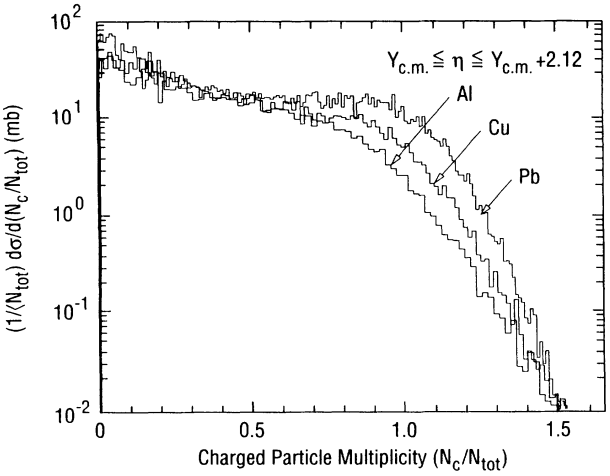

FIG. 18. $d\sigma/dN_c$ for a fixed interval in pseudorapidity relative to $Y_{c.m.}$ for each of the targets. The horizontal axis has been scaled by the maximum number of nucleons in the projectile-plus-target core as determined for each of the targets.

either a Si+Al or a Si+Cu collision. In Fig. 18 we show that the data do scale better (but not perfectly) with the total number of participant baryons, N_{tot}. Considering the simplicity of the assumptions used to calculate both T_f and N_{tot} it would be imprudent to derive more than general trends from Figs. 17 and 18.

V. CONCLUSIONS

The data presented here demonstrate a strong correlation between the transverse energy seen in the target calorimeter and the charged particle multiplicity seen in the multiplicity detector. The experimental results are well described by calculations using the HIJET event generator with inclusion of rescattering. The effect of rescattering is quite large for the Pb target. Correlations between N_c and E_0 further support the idea that substantial rescattering takes place in central Si+Pb collisions. Also the fact that substantially larger multiplicities (and TCAL E_t) are produced for the same amount of absorbed energy in Pb than in either Cu or Al leads one to the conclusion that the transverse energy per particle from a central Si+Pb collision must be smaller than that in either Si+Cu or Si+Al collisions. We have furthermore provided evidence that the multiplicity data reported here scale approximately in proportion to the total number of participant nucleons and that at AGS energies KNO scaling is satisfied. In general, the trend with target mass of the observed charged particle multiplicity distributions and their agreement with models which assume large amount of stopping and rescattering of produced particles lend additional, albeit indirect support to the interpretation that, in such collisions, zones of high particle and energy density may be formed.

ACKNOWLEDGMENTS

We especially acknowledge the Silicon Detector Group, headed by H.W. Kraner, in the BNL Instrumentation Division for their work in fabricating the unique silicon detectors used in this experiment and for their technical assistance. We acknowledge excellent support by the BNL AGS and Tandem staffs and thank Dr. Y. Makdisi and Dr. H. Brown for their expert help. John Sondericker III and R. Hutter provided much needed technical support. We acknowledge the assistance during the data taking and analysis by J. Dadusc (supported by the NSF Undergraduate Research Initiative Program). We would also like to thank Sergei Voloshin for useful discussions and suggestions. This research was supported, in part, by the U.S. DOE under Contract No. DEAC02-CH00016, the NSF, and the Natural Sciences and Engineering Research Council of Canada.

[1] J. Stachel, Nucl. Phys. **A525**, 23c (1991).
[2] M. Tincknell, in *Hadronic Matter in Collision 1988*, edited by P. Carruthers and J. Rafelski (World Scientific, Singapore, 1989), p. 378.
[3] H. Sorge *et al.*, Nucl. Phys. **A525**, 95c (1991).
[4] K. Werner, Z. Phys. C **38**, 193 (1988).
[5] B. Anderson, G. Gustafson, and B. Nilsson-Almqvist, Nucl. Phys. **B281**, 289 (1987).
[6] M. Gyulassy, CERN Report No. CERN-TH, 4794, 1987.
[7] A. Capella and J. Tran Than Van, Z. Phys. C **10**, 249 (1981); A. Capella *et al.*, *ibid.* **33**, 541 (1987).
[8] T. Ludlam, A. Pfoh, and A. Shor, Proceedings RHIC Workshop, BNL Report No. BNL–51921, 1985.
[9] J. Barrette *et al.*, E814 Collaboration, Phys. Rev. Lett. **64**, 1219 (1990).
[10] W. E. Cleland *et al.*, E814 Collaboration, Nucl. Phys. **A525**, 91c (1991).
[11] J. Fischer *et al.*, IEEE Trans. Nucl. Sci. **37**, 82 (1990).
[12] M. Fatyga, D. Makowiecki, and W. Llope, Nucl. Instrum. Methods Phys. **A284**, 323 (1989).
[13] J. Barrette *et al.*, E814 Collaboration, Phys. Rev. C **45**, 2427 (1992).
[14] R. Brun *et al.*, CERN Data Handling Division, Report No. DD/EE/84–1.
[15] R. H. Beuttenmuller *et al.*, Nucl. Instrum. Methods **A253**, 500 (1987).
[16] R. S. Longacre, in Proceedings of the Workshop on Heavy Ion Physics at the AGS, edited by Ole Hansen, BNL Report No. BNL-44911, 134 (1990); A. Shor and R. Longacre, Phys. Lett. B **218**, 100 (1989).
[17] J. Stachel and P. Braun-Munzinger, Phys. Lett. B **216**, 1 (1989); Nucl. Phys. **A498**, 577 (1989).
[18] L. Ramello *et al.*, HELIOS Collaboration, Nucl. Phys. **A525**, 555c (1991).
[19] P. Vincent *et al.*, E802 Collaboration, Nucl. Phys. **A498**, 67c (1989).
[20] S. Chapman and M. Gyulassy, Phys. Rev. Lett. **67**, 1210 (1991).
[21] T. Abbot *et al.*, E802 Collaboration, Phys. Rev. Lett. **64**, 847 (1990).
[22] Z. Koba, H. B. Nielson, and P. Olesen, Nucl. Phys. **B40**, 317 (1972).
[23] K. Sengupta, G. Singh, and P. L. Jain, Phys. Lett. **4B**, 548 (1988).
[24] A. Bialas, M. Bleszynski, and W. Czyz, Nucl. Phys. **B111**, 461 (1976).